Evaluating the low frequency predictions of a Boussinesq wave model: Field cases

James T. Kirby [1], *Qin Chen* [2], *T. James Noyes* [3], *Robert T. Guza* [3] *and Steve Elgar* [4]

1. Center for Applied Coastal Research, University of Delaware, Newark, DE 19716 USA

2. Department of Civil Engineering, University of South Alabama, Mobile, AL 36688 USA

3. Integrative Oceanography Division CCS 0209, Scripps Institution of Oceanography, La Jolla, CA 92093 USA

4. Applied Ocean Physics and Engineering, MS#11, Woods Hole Oceanographic Institution, Woods Hole, MA 02543 USA

ABSTRACT

Model results obtained using coupled wave-driver circulation models often provide poor reproduction of the frequency distribution of unsteady shear wave motions, in comparison to field data. In this study, we are examining the predictions of a Boussinesq model driven by irregular wave conditions derived from field data. Preliminary results indicate that the model predicts a much more energetic, irregular shear wave environment than is obtained in typical circulation models for similar incident wave conditions.

KEYWORDS : Nearshore hydrodynamics; wave breaking; surfzone processes; longshore currents; hydrodynamic instabilities

INTRODUCTION

Wave-driven currents on open coastal beaches can evolve into complex patterns with time and space scales that apparently differ from scales in the forcing mechanisms. Many of these patterns are explained at least qualitatively through the use of linear stability analysis of the initially smooth wave-driven circulation. One such motion that has drawn considerable attention is the so-called *shear wave*, which is thought to start as a wavy meander of the longshore current (Bowen and Holman, 1989) but which can grow into a variety of regular and chaotic patterns at finite amplitude (Allen et al, 1996). Field observations (Oltman-Shay et al, 1989, and subsequent work by many authors) indicate that motions of this general form are present in the field. The presence of these motions is illustrated graphically by means of a plot of power spectral density as a function of frequency and longshore wavenumber, as illustrated for the time period 0400-0700 on October 2, 1997 for the Sandyduck experiment (Noyes, 2002; Noyes et al, 2003a) in Figure 1. The presence of shear waves, which appear as a nondispersive motion at low frequency, is indicated by the ridge on the lower left in each panel.

Recent experience with coupled circulation/wave-driver models has indicated that unstable behavior of the wave-driven longshore current occurs for conditions corresponding to those at specific field sites, and that there is qualitative agreement between field and numerical data for the amplitude and spatial and

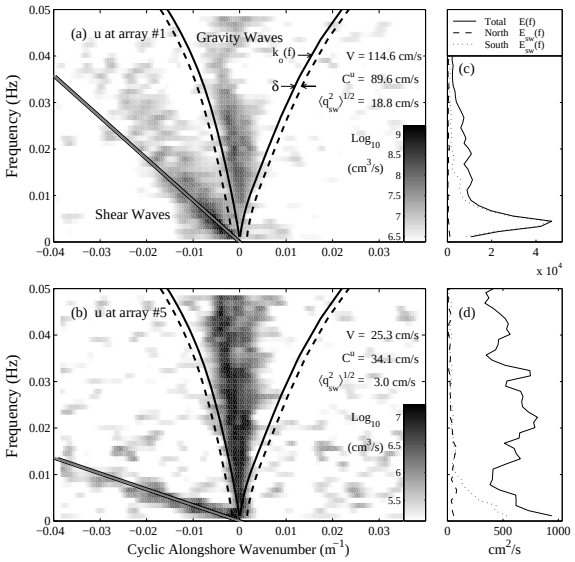

Figure 1: Left: Frequency-wavenumber spectra $E(k, f)$ of cross-shore velocity obtained at shallowest (a) $x = 160m$ and deepest (b) $x = 385m$ alongshore arrays, for 0400-0700 EST, 2 Oct. 1997. Shear waves are indicated by the straight-line fit at lower left in each plot, which represent motions outside the envelope of known gravity wave modes, indicated by the band enclosed by dashed curves. Right: Frequency spectra of northward propagating, southward propagating and total shear wave energy outside the gravity wave band. (From Noyes, 2002; Noyes et al 2003a).

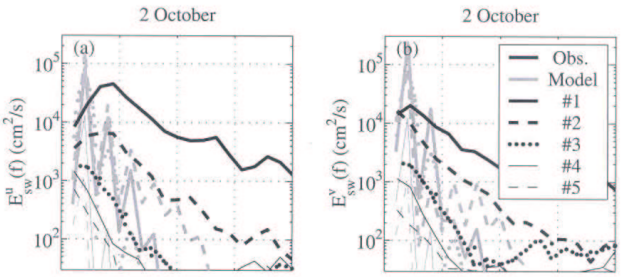

Figure 2: Observed (black) and modeled (gray) shear wave frequency spectra at the five cross-shore array locations in the Sandyduck field experiment. Left: cross-shore velocities. Right: longshore velocities. (from Noyes, 2002; Noyes et al 2003b).

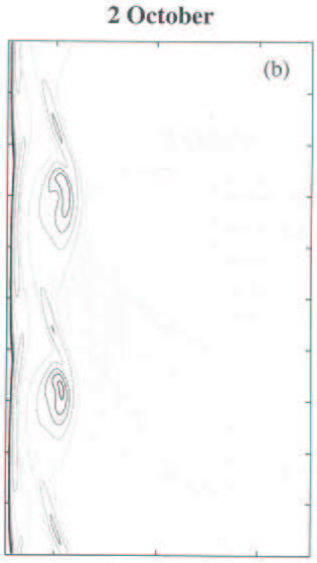

Figure 3: Contour plot of instantaneous vorticity $v_x - u_y$ for simulation of Oct. 2, 0400-0700 EST, 1997. Beach is on the left. (from Noyes, 2002; Noyes et al 2003b).

time scales of the unsteady motion, when reasonable choices for driving forces and frictional dissipation are used in the models (Özkan-Haller and Kirby, 1999; Noyes, 2002; Noyes et al, 2003b). However, there are still aspects of the results of this modeling approach which are unsatisfactory in the context of field observations. First, it has been observed (Özkan-Haller and Kirby, 1999; Noyes, 2002; Noyes et al, 2003b) that model results tend to indicate that unstable motions are most predominant at very low frequencies, and drop off rapidly with increase in frequency. In contrast, field data indicate that the power spectral density associated with the shear wave "ridge" remains more prominant with increasing frequency. It is apparent that the 2-D circulation models do not reproduce much of the finer scale, higher frequency and wavenumber portion of the complex flow field. This is not thought to be merely a problem with model resolution; convergence of results for cases from the Superduck experiment has been tested by Özkan-Haller and Kirby (1999) and found to be satisfactory. An illustration of the rapid roll-off in numerical results for spectral density is indicated in Figure 2 (Noyes, 2002; Noyes et al, 2003b), where a model similar to that of Allen et al (1996) has been used. The resulting flow field is fairly smooth and lacks small scale features. Figure 3 shows model computations (Noyes, 2002; Noyes et al, 2003b) of the pattern of vorticity for the resulting finite amplitude flow field, and shows that the motion predicted by the numerical model consists of well organized large scale rolls.

In this study, we are using the Boussinesq model of Wei et al (1995), Chen et al (2000), Kennedy et al (2000) and Chen et al (2003) to study the generation of low-frequency motions driven by obliquely incident, breaking surface waves on an open coastal beach. This paper describes the model being employed. A preliminary illustration of model results for the case of conditions from October 2, 1997, 0400-0700 EST during the Sandyduck field experiment is shown. Methods for extracting the vorticity field from instantaneous model results, and for reconstructing the corresponding rotational velocity field, are described. Comparisons between field data and model computations for this and additional time periods will be shown during the presentation.

THE MODEL

The Boussinesq model used here is based on the work of Wei et al (1995), who developed a model for inviscid, irrotational wave motion in a shallow layer over variable bathymetry in two horizontal dimensions. The development of the model follows the formalism of Nwogu (1993), who utilized horizontal velocities at a reference elevation z_α together with surface displacement η as dependent variables, but does not make any restrictions on the size of a parameter $\delta = a_0/h_0$ characterising nonlinearity. Further extensions to incorporate surfzone wave breaking and shoreline runup have been made by Kennedy et al (2000) and Chen et al (2000). Chen et al (2003) describe a modification to the model to account for proper treatment of the vertical component of vorticity in the nearly horizontal flow field. An overview of the model and it's application to nearshore processes may be found in Kirby (2003).

Hydrodynamic equations

Following Nwogu (1993), we define a reference elevation z_α located within the water column, and express the series expansion for the velocity potential ϕ in terms of the value at z_α. Truncating the resulting series after $O(\mu^2)$ (where μ characterizes the ratio of water depth to wavelength) gives

$$\begin{aligned}\phi(x,y,z,t) &= \phi_\alpha(x,y,t) + \mu^2(z_\alpha - z)\nabla\cdot(h\nabla\phi_\alpha) \\ &\quad -\frac{1}{2}\mu^2({z_\alpha}^2 - z^2)\nabla^2\phi_\alpha + O(\mu^4) \qquad (1)\end{aligned}$$

When used in the linearized free surface boundary conditions, the form (1) corresponds to a dispersion relation given by

$$\omega^2 = gk^2h\frac{1-(\alpha+1/3)(kh)^2}{1-\alpha(kh)^2} \qquad (2)$$

where

$$\alpha = \frac{1}{2}\left(\frac{z_\alpha}{h}\right)^2 + \frac{z_\alpha}{h} \tag{3}$$

The choice of α fixes the resulting dispersion relation and the corresponding value of z_α. $\alpha = -1/3$ reproduces the classical Boussinesq theory based on depth-averaged velocity, while the choice $\alpha = -2/5$ reproduces a $(2,2)$ Padé approximant of the full linear dispersion relation.

An expression for the horizontal velocity vector at depth z_α follows from

$$\nabla\phi_\alpha = \mathbf{u}_\alpha - \mu^2[\nabla z_\alpha \nabla\cdot(h\mathbf{u}_\alpha) + z_\alpha \nabla z_\alpha \nabla\cdot\mathbf{u}_\alpha] + O(\mu^4) \tag{4}$$

We obtain an equation for mass conservation from the depth-integrated continuity equation

$$\eta_t + \nabla\cdot\mathbf{M} = 0; \qquad \mathbf{M} = \int_{-h}^{\delta\eta} \nabla\phi dz \tag{5}$$

and get

$$\begin{aligned}\mathbf{M} &= H\left[\mathbf{u}_\alpha\right. \\ &+ \mu^2\left\{\left[\frac{1}{2}{z_\alpha}^2 - \frac{1}{6}(h^2 - h\delta\eta + (\delta\eta)^2)\right]\nabla(\nabla\cdot\mathbf{u}_\alpha)\right. \\ &+ \left.\left.\left[z_\alpha + \frac{1}{2}(h-\delta\eta)\right]\nabla(\nabla\cdot(h\mathbf{u}_\alpha))\right\}\right] + O(\mu^4)\end{aligned} \tag{6}$$

for volume flux, where H is total water depth $h + \delta\eta$.

Taking the horizontal gradient of the Bernoulli equation evaluated at z_α gives a corresponding horizontal momentum equation, given by

$$\mathbf{u}_{\alpha t} + \delta(\mathbf{u}_\alpha\cdot\nabla)\mathbf{u}_\alpha + \nabla\eta + \mu^2\mathbf{V_1} + \delta\mu^2\mathbf{V_2} = O(\mu^4) \tag{7}$$

with

$$\begin{aligned}\mathbf{V_1} &= \frac{1}{2}{z_\alpha}^2\nabla(\nabla\cdot\mathbf{u}_{\alpha t}) + z_\alpha\nabla(\nabla\cdot(h\mathbf{u}_{\alpha t})) \\ &\quad -\nabla\left[\frac{1}{2}(\delta\eta)^2\nabla\cdot\mathbf{u}_{\alpha t} + \delta\eta\nabla\cdot(h\mathbf{u}_{\alpha t})\right]\end{aligned} \tag{8}$$

$$\begin{aligned}\mathbf{V_2} &= \nabla\left[(z_\alpha - \delta\eta)(\mathbf{u}_\alpha\cdot\nabla)(\nabla\cdot(h\mathbf{u}_\alpha))\right. \\ &\quad \left.+\frac{1}{2}({z_\alpha}^2 - (\delta\eta)^2)(\mathbf{u}_\alpha\cdot\nabla)(\nabla\cdot\mathbf{u}_\alpha)\right] \\ &\quad +\frac{1}{2}\nabla\left[(\nabla\cdot(h\mathbf{u}_\alpha) + \delta\eta\nabla\cdot\mathbf{u}_\alpha)^2\right] \\ &\quad (\mathbf{u}_\alpha\cdot\nabla z_\alpha)\left[z_\alpha\nabla(\nabla\cdot\mathbf{u}_\alpha) + \nabla(\nabla\cdot(h\mathbf{u}_\alpha))\right] \\ &\quad -\nabla z_\alpha(\mathbf{u}_\alpha\cdot\nabla)(\nabla\cdot(h\mathbf{u}_\alpha)) \\ &\quad -z_\alpha\nabla z_\alpha(\mathbf{u}_\alpha\cdot\nabla)(\nabla\cdot\mathbf{u}_\alpha)\end{aligned} \tag{9}$$

as obtained by Chen et al (2003). Chen et al demonstrate that the resulting equations consistently conserves the vertical component of vorticity in an arbitrary flow to $O(\mu^2)$.

Wave breaking and shoreline conditions

The wave breaking model used here is based on the work of Zelt (1991), who provided an eddy viscosity model applied in a 1-D horizontal model. Extended to 2-D, the breaking wave force term $\mathbf{R_b}$ can be written as

$$\begin{aligned}R_b^x &= \frac{1}{H}\left(\{\nu_b[Hu_\alpha]_x\}_x\right. \\ &\quad \left.+\frac{1}{2}\{\nu_b[Hu_\alpha]_y + \nu_b[Hv_\alpha]_x\}_y\right)\end{aligned} \tag{10}$$

$$\begin{aligned}R_b^y &= \frac{1}{H}\left(\{\nu_b[Hv_\alpha]_y\}_y\right. \\ &\quad \left.+\frac{1}{2}\{\nu_b[Hv_\alpha]_x + \nu_b[Hu_\alpha]_y\}_x\right)\end{aligned} \tag{11}$$

Following Zelt (1991), Kennedy et al (2000) give the breaking wave eddy viscosity as

$$\nu_b = B\delta_b^2 H\eta_t \tag{12}$$

where δ_b is a mixing length coefficient which is calibrated to a value of 1.2. The coefficient B is used to turn the breaking term off or on depending on a criterion based on the vertical velocity of the surface. Again, following Zelt but using time derivatives in place of space derivatives, Kennedy et al used

$$B = \begin{cases} 1, & \eta_t \geq 2\eta_t^* \\ \frac{\eta_t}{\eta_t^*} - 1, & \eta_t^* < \eta_t \leq 2\eta_t^* \\ 0, & \eta_t \leq \eta_t^* \end{cases} \tag{13}$$

The parameter η_t^* determines the onset and cessation of breaking. Zelt (1991) chose this criterion to have a constant value, but Kennedy et al (2000) use a model for the parameter which involves a time history in order to allow the slope of the breaking wave crest to relax after the onset of breaking. The relationship is

$$\eta_t^* = \begin{cases} \eta_t^{(F)}, & t \geq T^* \\ \eta_t^{(I)} + \frac{t-t_0}{T^*}(\eta_t^{(F)} - \eta_t^{(I)}), & 0 \leq t - t_0 < T^* \end{cases} \tag{14}$$

Here, T^* is the elapsed time since the onset of the local breaking event, and the initiation and relaxed critical surface velocities are given by $\eta_t^{(I)} = 0.65\sqrt{gh}$ and $\eta_t^{(F)} = 0.15\sqrt{gh}$. In 2-D applications, the relationship must be augmented with a tracking algorithm to follow events along rays; see Chen et al (2000).

Moving shoreline conditions are treated using the slot method of Tao (1984), in which deep, narrow, flooded slots are added to each grid row, extending down at least to the lowest elevation that will be experienced during shoreface rundown. Kennedy et al (2000) modified the method to better enforce mass conservation.

Bottom friction and subgrid mixing effects

Since the velocity field in a Boussinesq calculation resolves the instantaneous wave orbital motion, the choice of a bottom friction formulation is relatively straightforward, and is given by

$$\mathbf{R_f} = \frac{f}{H}|\mathbf{u}_\alpha|\mathbf{u}_\alpha \tag{15}$$

where the friction factor is on the order of 10^{-3} in most simulations (Chen et al, 2003). Note that the term is written in terms of the reference velocity $\mathbf{u}_\alpha$ rather than the bottom velocity, which would tend to reduce the size of f somewhat.

Nearshore current systems are affected by several lateral mixing effects, including both turbulent mixing and lateral shear dispersion resulting from the three-dimensional structure of real currents and their interaction with the wave orbital velocity. Of these, the shear dispersion can be an order of magnitude larger (Svendsen and Putrevu, 1994), and an attempt has been made to incorporate it's effect in most of our nearshore simulations. Chen et al (1999) formulate the effect as a Smagorinsky subgrid model with the form

$$R_s^x = \frac{1}{H}\left(\{\nu_s[Hu_\alpha]_x\}_x + \frac{1}{2}\{\nu_s[Hu_\alpha]_y + \nu_s[Hv_\alpha]_x\}_y\right) \quad (16)$$

$$R_s^y = \frac{1}{H}\left(\{\nu_s[Hv_\alpha]_y\}_y + \frac{1}{2}\{\nu_s[Hv_\alpha]_x + \nu_s[Hu_\alpha]_y\}_x\right) \quad (17)$$

where ν_s is an eddy viscosity arising from the mean flow field,

$$\nu_s = c_m \Delta x \Delta y \left[(U_x)^2 + (V_y)^2 + \frac{1}{2}(U_y + V_x)^2\right]^{1/2} \quad (18)$$

and where U and V are suitable time averages of the velocity field. Chen et al (1999) and subsequent studies have used time averages over two wave periods for regular waves or over ten peak wave periods for irregular waves, and typically use $c_m = 0.25$. Although Chen et al (2003) provide some discussion on the choice of this parameter, this aspect of the model application has not been extensively evaluated.

Numerical method

Wei and Kirby (1995) have described a numerical scheme for equations of this type which has come into fairly wide usage. Time stepping is treated using a fourth-order Adams-Bashforth-Moulton scheme, while spatial differencing is handled using a mixed-order scheme, employing fourth-order accurate centered differences for first derivatives and second-order accurate derivatives for third derivatives. The latter choice is made in order to move leading truncation errors to one order higher than the $O(\mu^2)$ dispersive terms, while maintaining the tridiagonal structure of spatial derivatives within time-derivative terms. Wei and Kirby (1995) used a non-staggered grid scheme with $\mathbf{u}_\alpha$ and η defined at the same locations. The method of Wei et al (1999) for generating waves at internal sources has been extended to the case of a periodic domain by Chen et al (2003). Kirby et al (1998) document a version of the non-staggered code, known as *FUNWAVE*, which is available at http://chinacat.coastal.udel.edu/∼kirby/programs/funwave.

APPLICATION TO SANDYDUCK EXPERIMENT

The model described above is presently being used in a study of shear waves during the Sandyduck field experiment in 1997 at Duck, North Carolina, USA. Results for the time period 0400-0700 EST, Oct. 2 are illustrated here. Model bathymetry is constructed from a composite of high resolution minigrid data for a time close to the interval in question, and an interpolation between the two larger-area CRAB surveys which bracket the study time. Figure 4 shows the bathymetry and instrument locations in local FRF coordinates, with x oriented offshore and y directed alongshore in the northerly direction. A cross-shore transect of the bathymetry together with an indication of the cross-shore location of the longshore instrument arrays is provided in the top panel of Figure 5.

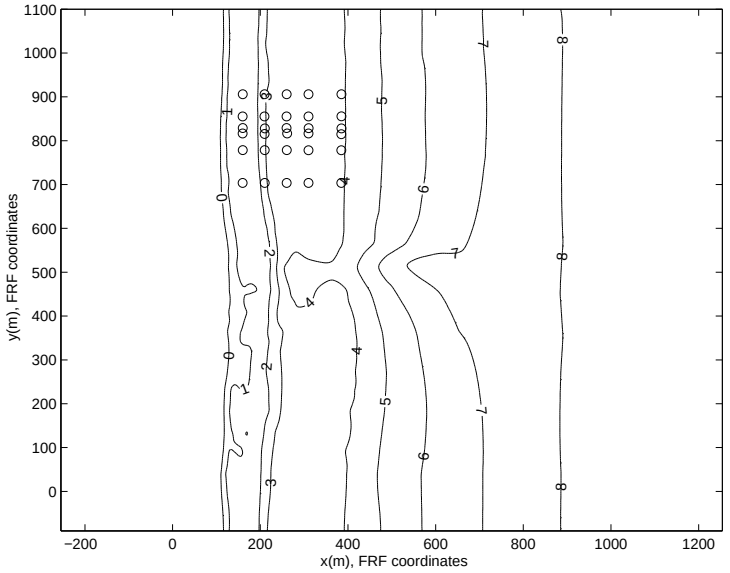

Figure 4: Model bathymetry for October 2 simulation. Depression in center of grid is the scour hole under the FRF pier. Instrument arrays extend from $y = 700m$ to $900m$ alongshore and from $x = 160m$ to $384m$ cross-shore. Circles denote instrument locations in the five principal longshore arrays.

Input wave conditions for model runs are derived from published frequency-direction spectra which are available on the FRF web site. These data are mapped onto a grid of allowable longshore wavenumbers and then utilized in a computation with enforced longshore periodicity. Realizations of 3.5 hour duration are constructed using linear superposition of directional components and random phases. A snapshot of a resulting water surface is shown in relation to the instrument array in the lower panel of Figure 5.

Extraction of low-frequency motion

In a study of numerical simulations of rip current dynamics and instabilities, Chen et al (1999) found that vorticity values computed using either the instantaneous reference velocity $\mathbf{u}_\alpha$ or an averaged velocity viewed through a window several wave periods long were virtually identical, aside from some signature of the incident wave associated with strong velocities under wave crests. This result indicated that the bulk of the wave-induced motion in the horizontal plane remains irrotational, even in the presence of an underlying rotational current field. In this study, we are using

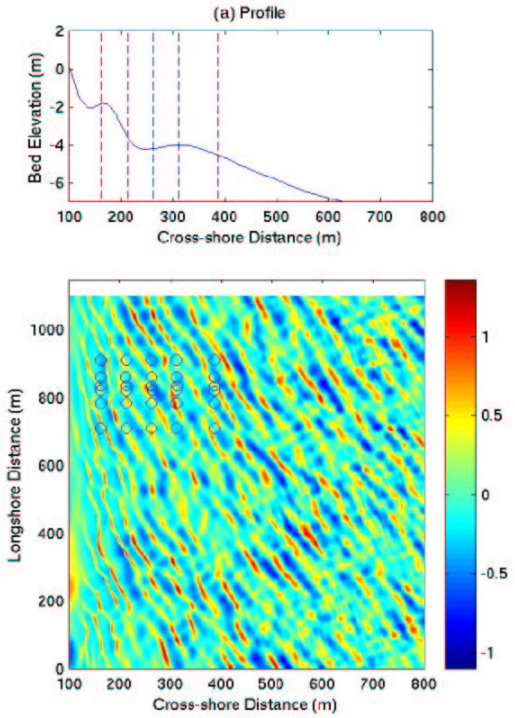

Figure 5: Upper panel: Bathymetry profile through center of instrument array, showing two longshore bar features. Dashed lines indicate the cross-shore location of longshore instrument arrays.

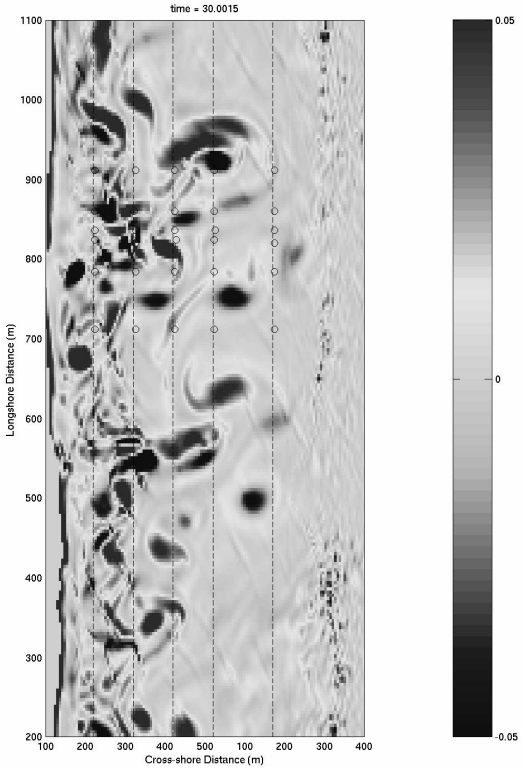

Figure 6: Snapshot of vertical vorticity derived from instantaneous Boussinesq velocities. 0400-0700 EST, Oct. 2. Compare with results in Figure 3, obtained using a coupled wave-driver/circulation model.

the instantaneous vertical vorticity computed by

$$\omega_z = v_{\alpha,x} - u_{\alpha,y} \tag{19}$$

as an indicator of the wave-driven rotational current field. A snapshot of the vorticity field derived this way for a time 30 minutes into the simulation of the 0400-0700 period is shown in Figure 6. This condition corresponds to the same average forcing conditions as for Figure 3, and it is clear that the vorticity field produced by the Boussinesq model is more energetic and contains a great deal more fine structure. In this picture, the longshore current is flowing from top to bottom in the picture, and the locations of the 5 longshore arrays are indicated.

Analysis of the frequency-longshore wavenumber structure of the vorticity field is based on time stacks of vorticity taken from the spatial vorticity images at the cross-shore locations of arrays 1, 2 and 5, indicated in Figures 5 and 6. The time stacks are illustrated in Figures 7-9. Figure 7 shows the vorticity structure in the trough region landward of the shore-parallel bar, and indicates a wide range of active frequencies as well as an indication of variations in longshore advection speed of the flow structures (indicated by the slope of diagonal structures in the figure), which typically is lower for prominant large scale features which span a wider cross-shore distance.

Just offshore of the bar crest, Figure 8 shows less small-scale structure and a predominance of the more energetic features also seen in Figure 7, indicating that these flow features span the two inshore arrays and are either moving as a coherent wave form or are being advected as coherent features by the longshore current.

In contrast, Figure 9 indicating results offshore at array 5, shows the presence of structures which are not moving only slowly in the longshore direction, suggesting that these represent eddies which have been shed to the offshore region and which are phase-decoupled from any organized wave-like motion in the surfzone and are stationary due to the absence of a background longshore current. These results are qualitatively consistant with the lower panel in Figure 1, where the apparent longshore phase speed of the shear wave ridge is significantly lower than in the top panel, for the inshore array.

Reconstructing the rotational velocity field

We are examining reconstructed velocity fields which are obtained using a stream function formulation. Letting

$$u_\alpha = -\psi_y; \qquad v_\alpha = \psi_x \tag{20}$$

and cross-differentiating gives Poisson's equation

$$\psi_{xx} + \psi_{yy} = \omega_z \tag{21}$$

This equation is solved with periodic boundary conditions in y using Fourier methods, and by second-order finite differences in

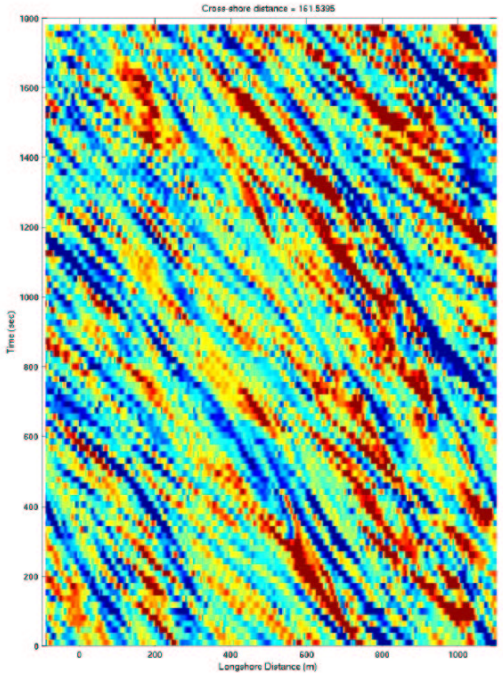

Figure 7: Time stack of model simulation of vorticity at longshore array 1, 0400-0700 EST, Oct. 2.

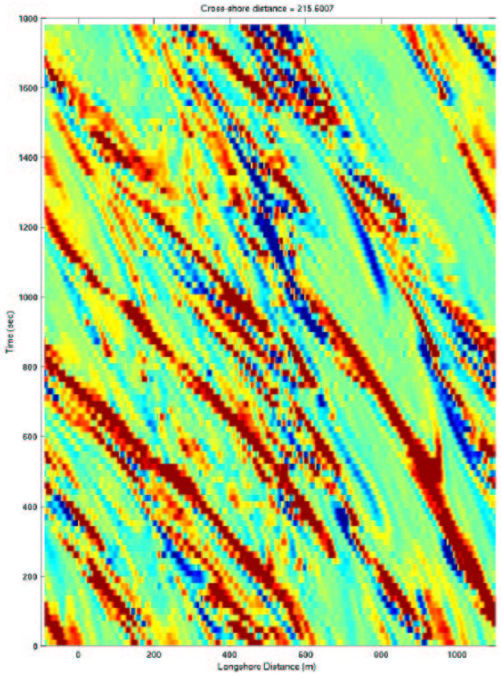

Figure 8: Time stack of model simulation of vorticity at longshore array 2, 0400-0700 EST, Oct. 2.

the cross-shore direction. Boundary conditions are chosen to be $\psi = 0$ onshore and $\psi_x = 0$ offshore. The offshore condition could fail if an energetic eddy drifted out to the offshore boundary, but this has not been found to be a problem and the method appears to be robust in preliminary analyses. After determining ψ, the rotational velocity field is recovered using (20).

CONCLUSIONS

Results to date indicate that the Boussinesq model predicts a low frequency flow field that is qualitatively similar to the types of flow fields generated by coupled wave-drivercirculation models. For given values of incident wave conditions and bottom friction coefficient, the low frequency flow field generated in the Boussinesq code is relatively more energetic and complex than the related fields generated in circulation models, with more fine structure and more active eddy shedding. These flow fields are presently being compared with field data, and additional days from the experiment are being examined. Results of the analysis will be discussed during the presentation.

ACKNOWLEDGMENT

This research is supported by the National Ocean Partnership Program (NOPP), grant N00014-99-1-1051 to the University of Delaware. Mr. Junwoo Choi graciously provided his bathymetry grid. The Office of Naval Research supported collection of field data.

REFERENCES

Allen, J. S., Newberger, P. A. and Holman, R. A., 1996, "Nonlinear shear instabilities of alongshore currents on plane beaches", *J. Fluid Mech.*, **310**, 181-213.

Bowen, A. J. and Holman, R. A., 1989, "Shear instabilities of the mean longshore current. 1. Theory", *J. Geophys. Res.*, **94**, 18,023-18,030.

Chen, Q., Dalrymple, R. A., Kirby, J. T., Kennedy, A. B. and Haller, M. C., 1999, "Boussinesq modeling of a rip current system", *J. Geophys. Res.*, **104**, 20,617 - 20,637.

Chen, Q., Kirby, J. T., Dalrymple, R. A., Kennedy, A. B. and Chawla, A., 2000, "Boussinesq modeling of wave transformation, breaking and runup. II: 2D", *J. Waterway, Port, Coastal and Ocean Engineering*, **126**, 48-56.

Chen, Q., Kirby, J. T., Dalrymple, R. A., Shi, F. and Thornton, E. B., 2003, "Boussinesq modeling of longshore currents", submitted to *J. Geophys. Res.*

Kennedy, A.B., Chen, Q., Kirby, J.T. and Dalrymple, R. A., 2000, "Boussinesq modeling of wave transformation, breaking, and runup. I: 1D," *J. Waterway Port Coastal and Ocean Engng.*, **126**, 39-47.

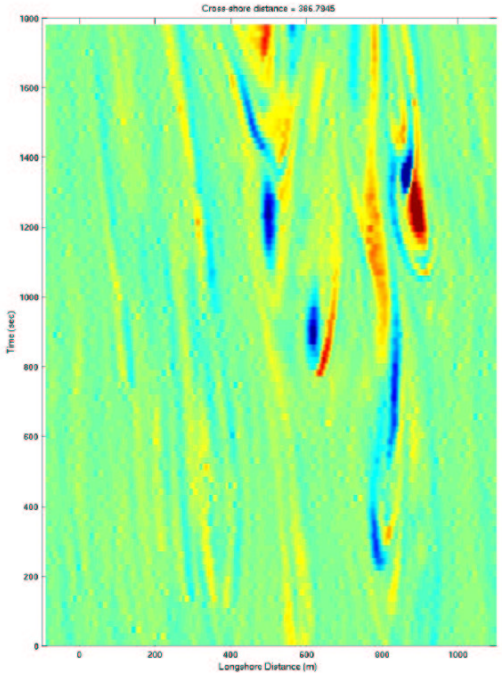

Figure 9: Time stack of model simulation of vorticity at longshore array 5, 0400-0700 EST, Oct. 2.

Kirby, J. T., Wei, G., Chen, Q., Kennedy, A. B. and Dalrymple, R. A., (1998), " FUNWAVE 1.0. Fully nonlinear Boussinesq wave model. Documentation and user's manual", Report CACR-98-06, Center for Applied Coastal Research, Department of Civil and Environmental Engineering, University of Delaware.

Kirby, J. T., 2003, "Boussinesq models and applications to nearshore wave propagation, surfzone processes and wave-induced currents", to appear in *Advances in Coastal Engineering*, V. C. Lakhan (ed), Elsevier Press.

Noyes, T. J., 2002, "Field observations of shear waves", Ph.D. thesis, Scripps Institution of Oceanography, La Jolla.

Noyes, T. J., Guza, R. T., Elgar, S. and Herbers, T. H. C., 2003a, "Field observations of shear waves in the surfzone", submitted to *J. Geophys. Res.*

Noyes, T. J., Guza, R. T., Elgar, S. and Herbers, T. H. C., 2003b, "Comparison of observed shear waves with numerical simulations", in preparation.

Nwogu, O., 1993, ""Alternative form of Boussinesq equations for nearshore wave propagation", *J. Waterway, Port, Coast. and Ocean Engrng.*, **119**, 618-638.

Oltman-Shay, J., Howd, P. A. and Birkemeier, W. A., 1989, "Shear instabilities of the mean longshore current. 2. Field observations", *J. Geophys. Res.*, **94**, 18,031-18,042.

Özkan-Haller, H. T. and Kirby, J. T., 1999, "Nonlinear evolution of shear instabilities of the longshore current: a comparison of observations and computations", *J. Geophys. Res.*, **104**, 25,953-25,984.

Svendsen, I. A. and Putrevu, U., 1994, "Nearshore mixing and dispersion", *Proc. Roy. Soc. London A*, **445**, 1-16.

Tao, J., 1984, "Numerical modelling of wave runup and breaking on the beach", *Acta Oceanologica Sinica*, **6**, 692-700 (in Chinese).

Wei, G. and Kirby, J. T., 1995,"A time-dependent numerical code for extended Boussinesq equations", *J. Waterway, Port, Coastal and Ocean Engrng.*, **120**, 251-261.

Wei, G., Kirby , J.T, Grilli, S.T. and Subramanya, R., 1995, "A fully nonlinear Boussinesq model for surface waves. Part 1. Highly nonlinear unsteady waves", *J. Fluid Mech.*, **294**, 71-92.

Wei, G., Kirby, J. T. and Sinha, A., 1999, "Generation of waves in Boussinesq models using a source function method", *Coastal Engnrng.*, **36**, pp. 271-299.

Zelt, J. A., 1991, "The runup of nonbreaking and breaking solitary waves", *Coastal Engineering*, **15**, 205-246.